

# Simulation-Prior Independent Neural Unfolding Procedure

Anja Butter<sup>1,2</sup>, Theo Heimel<sup>3</sup>, Nathan Huetsch<sup>1</sup>, Michael Kagan<sup>4</sup>, and Tilman Plehn<sup>1,5</sup>

<sup>1</sup> Institut für Theoretische Physik, Universität Heidelberg, Germany

<sup>2</sup> LPNHE, Sorbonne Université, Université Paris Cité, CNRS/IN2P3, Paris, France

<sup>3</sup> CP3, Université catholique de Louvain, Louvain-la-Neuve, Belgium

<sup>4</sup> SLAC National Accelerator Laboratory, Menlo Park, CA, USA

<sup>5</sup> Interdisciplinary Center for Scientific Computing (IWR), Universität Heidelberg, Germany

July 22, 2025

## Abstract

Machine learning allows unfolding high-dimensional spaces without binning at the LHC. The new SPINUP method extracts the unfolded distribution based on a neural network encoding the forward mapping, making it independent of the prior from the simulated training data. It is made efficient through neural importance sampling, and ensembling can be used to estimate the effect of information loss in the forward process. We showcase SPINUP for unfolding detector effects on jet substructure observables and for unfolding to parton level of associated Higgs and single-top production.

---

## Contents

<b>1</b>	<b>Introduction</b>	<b>2</b>
<b>2</b>	<b>Forward unfolding</b>	<b>3</b>
2.1	Neural Empirical Bayes	3
2.2	SPINUP	4
<b>3</b>	<b>Gaussian illustration</b>	<b>7</b>
<b>4</b>	<b>Jet substructure dataset</b>	<b>9</b>
<b>5</b>	<b>Unfolding to parton level</b>	<b>12</b>
5.1	Unfolding	13
5.2	Inference	14
5.3	Lower data statistic	18
<b>6</b>	<b>Outlook</b>	<b>18</b>
<b>A</b>	<b>Hyperparameters</b>	<b>20</b>
<b>B</b>	<b>Additional results</b>	<b>21</b>
	<b>References</b>	<b>23</b>

---

# 1 Introduction

The vast data volumes and high-precision simulations at the LHC offer a unique opportunity to address some of the most fundamental questions in particle physics. At the same time, they present a challenge to our capacity for data analysis. Monte Carlo generators form a robust foundation for simulation-based inference, modeling the full range of physics effects, from the hard scattering through parton showering and hadronization, all the way to the detector response [1, 2]. However, the overall computational cost of these simulations is already high, and projected to grow beyond available computational resources with the upcoming HL-LHC.

This motivates an alternative analysis strategy, based on data representations removing the detector or other, low-energy aspects of the forward simulation: (i) once unfolded, data can be used to test any number of new physics model very economically; (ii) unfolded data can be used by a broad physics community, not just inside the established collaborations. As a side effect, unfolded data from different experiments can be combined for instance for global SMEFT analyses [3, 4], to answer the question to what level LHC data as a whole is described by the Standard Model.

Unfolding traditionally relied on matrix based approaches [5, 6]. While providing precise and accurate results when unfolding data represented as one dimensional histograms, such binned approaches do not work for many dimensions. Unfolding methods based on machine learning [2, 7] open up new ways to perform unbinned and multi-dimensional cross section measurements [7]. These unfolding methods mainly rely either on classifier based approaches [8] or generative neural networks [9]. Classifiers can reweight a Monte Carlo simulation to the true underlying distribution [8, 10]. Generative network can either learn a direct mapping between distributions at reco and truth level [11–15] or learn a probability distribution at truth level for each reco level event [9, 16–22]. A comparison of different generative approaches can be found in Ref. [23].

While ML-unfolding lifts the restriction to low dimensional methods, some challenges of matrix based unfolding remain, in particular the impact of the simulation bias on unfolded data. Traditional unfolding techniques mitigate this prior dependence through Iterative Bayesian Unfolding [24, 25]. Alternative approaches regularize the inversion matrix using singular value decomposition [26] or Tikhonov regularization [27]. ML-approaches adapt iterative approaches [8, 18, 28], as well as bias reducing data processing techniques [29] which have been shown to work in experimental settings [29–34]. The disadvantage of iterative methods is that they are not data-efficient.

We explore a one-step approach to avoiding this bias in our Simulation-Prior Independent Neural Unfolding Procedure (SPINUP). It builds on the Neural Empirical Bayes (NEB) [17] approach and encodes the unfolded distribution as a generative model that can be forward-mapped to match the observed data. The unfolded distribution is then found by minimizing the difference between the folded distribution at the reconstruction level and the observed data. We develop a new ML-approach including importance sampling and pretraining. It alleviates the high computational cost associated with integrating the likelihood in every training step, and allows the method to scale to more challenging problems. We also show how ensembling tracks the unfolding uncertainty from the loss of information in the forward process.

In this paper we first present the method and our extensions in Sec. 2. We then use a Gaussian toy example to showcase our method and the effect of ensembling in Sec. 3. In Sec. 4 we apply SPINUP to the Omnifold jet substructure dataset [8], an established unfolding benchmark. Finally, as a challenging physics example we unfold the full phase space of  $tHj$  events to parton level. Here, we demonstrate how SPINUP recovers the parton-level distribution to high precision, without showing any prior dependence, and allows to measure the CP-phase

in the top Yukawa coupling from unfolded data [35–43].

## 2 Forward unfolding

We can understand unfolding using four probabilities, the simulated part-level distribution\*, the simulated reco-level distribution, the measured reco-level distribution in data, and the unfolded part-level distribution. They are related as [44]

$$\begin{array}{ccc}
 p_{\text{sim}}(x_{\text{part}}) & \xleftrightarrow{\text{unfolding inference}} & p_{\text{unfold}}(x_{\text{part}}) \\
 \downarrow p(x_{\text{reco}}|x_{\text{part}}) & & \uparrow \text{unfold} \\
 p_{\text{sim}}(x_{\text{reco}}) & \xleftrightarrow{\text{forward inference}} & p_{\text{data}}(x_{\text{reco}})
 \end{array} \quad (1)$$

The density  $p(x_{\text{reco}}|x_{\text{part}})$  describes the forward mapping from the part-level phase space to the reco-level phase space. It is encoded implicitly in simulators in the form of paired events in  $x_{\text{part}}$  and  $x_{\text{reco}}$ . Like all unfolding methods, we assume that  $p(x_{\text{reco}}|x_{\text{part}})$  is correctly described by the simulators.

Phrasing the problem in terms of our forward unfolding method, we want to find a distribution in  $x_{\text{part}}$  that reproduces  $p_{\text{data}}(x_{\text{reco}})$  once it is folded with the forward mapping. Typically, there is no unique unfolding solution, because limited statistics and information loss in the forward mapping can lead to a range of valid  $p_{\text{unfold}}(x_{\text{part}})$  solutions.

### 2.1 Neural Empirical Bayes

We can solve this unfolding problem in a forward fashion, building on the Neural Empirical Bayes (NEB) approach [17]. Here, we encode the forward mapping  $p(x_{\text{reco}}|x_{\text{part}})$  and the unfolded distribution  $p_{\text{unfold}}(x_{\text{part}})$  in generative neural networks and train the latter to reproduce  $p_{\text{data}}(x_{\text{reco}})$ .

**Unfolding network** The central object in forward unfolding is the generative network

$$p_{\theta}(x_{\text{part}}) \approx p_{\text{unfold}}(x_{\text{part}}), \quad (2)$$

for which we adapt the parameters until the resulting reco-level distribution matches the data,

$$p_{\theta}(x_{\text{reco}}) = \int dx_{\text{part}} p(x_{\text{reco}}|x_{\text{part}}) p_{\theta}(x_{\text{part}}) \stackrel{!}{=} p_{\text{data}}(x_{\text{reco}}). \quad (3)$$

For a valid solution, the folded distribution has to agree with the data. The loss quantifies the discrepancy between these two reco-level distributions,

$$D_{\text{KL}}[p_{\text{data}}(x_{\text{reco}}), p_{\theta}(x_{\text{reco}})] = - \underbrace{\int dx_{\text{reco}} p_{\text{data}}(x_{\text{reco}}) \log p_{\theta}(x_{\text{reco}})}_{\equiv \mathcal{L}} + \text{const}. \quad (4)$$

where

$$\log p_{\theta}(x_{\text{reco}}) = \log \int dx_{\text{part}} p_{\theta}(x_{\text{part}}) p(x_{\text{reco}}|x_{\text{part}}). \quad (5)$$

Minimizing the KL-divergence with respect to  $\theta$  is equivalent to maximizing the log-likelihood of the observed data distribution  $p_{\text{data}}(x_{\text{reco}})$  under our unfolding model  $p_{\theta}(x_{\text{part}})$ .

\*We use the term part-level to cover unfolding to particle level and to parton level.

**Transfer network** The main challenge of forward unfolding is the calculation of  $p_\theta(x_{\text{reco}})$  in Eq.(5) using the forward mapping  $p(x_{\text{reco}}|x_{\text{part}})$ . Standard simulators encode this density implicitly. To access it explicitly, we use paired simulated data  $(x_{\text{part}}, x_{\text{reco}}) \sim P_{\text{sim}}(x_{\text{part}}, x_{\text{reco}})$  to train a conditional generative neural network [17, 45, 46] ahead of time,

$$p_\varphi(x_{\text{reco}}|x_{\text{part}}) \approx p(x_{\text{reco}}|x_{\text{part}}). \quad (6)$$

During the training of the unfolding network  $p_\theta(x_{\text{part}})$ , the transfer network  $p_\varphi(x_{\text{reco}}|x_{\text{part}})$  is frozen. In the following we will drop the subscript  $\varphi$ .

**Monte Carlo integration** The loss evaluation in Eq.(4) uses mini-batches. Following Eq.(5) we rely on Monte Carlo integration, for each sample  $x_{\text{reco}} \sim p_{\text{data}}(x_{\text{reco}})$ , to calculate

$$\begin{aligned} \log p_\theta(x_{\text{reco}}) &= \log \int dx_{\text{part}} p_\theta(x_{\text{part}}) p(x_{\text{reco}}|x_{\text{part}}) \\ &= \lim_{N_{\text{MC}} \rightarrow \infty} \log \frac{1}{N_{\text{MC}}} \sum_{\{x_{\text{part}}\}}^{N_{\text{MC}}} p(x_{\text{reco}}|x_{\text{part}}) \Big|_{x_{\text{part}} \sim p_\theta(x_{\text{part}})}. \end{aligned} \quad (7)$$

The algorithm samples a batch of points from  $p_\theta(x_{\text{part}})$  and passes them through the transfer network to estimate  $\log p(x_{\text{reco}}|x_{\text{part}})$ . These are aggregated using the numerically stable logsumexp operation

$$\log p_\theta(x_{\text{reco}}) = \text{logsumexp} \left( p(x_{\text{reco}}|x_{\text{part}, 1}), \dots, p(x_{\text{reco}}|x_{\text{part}, N_{\text{MC}}}) \right) - \log N_{\text{MC}}. \quad (8)$$

Since the integration is inside of the log, the MC approximation of the integral is also inside the log. This results in a biased but consistent estimator for the marginal log likelihood, with the bias rapidly decreasing towards zero as  $N_{\text{MC}}$  increases [17].

## 2.2 SPINUP

Our Simulation-Prior Independent Neural Unfolding Procedure (SPINUP) uses state-of-the-art generative ML for the forward unfolding described above. Challenges arise when the transfer function  $p(x_{\text{reco}}|x_{\text{part}})$  has narrow peaks. This increases the variance in the Monte Carlo samples and renders a poor integral estimate. Increasing the number of Monte Carlo samples is not a scalable solution, because evaluating the loss from Eq.(7) on a batch of reco-level events involves calculating the transfer probability for each reco-part pairing, so the memory cost is proportional to  $N_{\text{Batch}} \times N_{\text{MC}}$ .

**Neural importance sampling** To improve the integration we employ neural importance sampling (NIS) [47–49], similar to Refs. [45, 46]. It encodes a suitable importance sampling  $q(x_{\text{part}}|x_{\text{reco}})$  in a generative network to compute the integral in Eq.(5)

$$\log p_\theta(x_{\text{reco}}) = \log \int dx_{\text{part}} q(x_{\text{part}}|x_{\text{reco}}) \frac{p_\theta(x_{\text{part}}) p(x_{\text{reco}}|x_{\text{part}})}{q(x_{\text{part}}|x_{\text{reco}})}. \quad (9)$$

Choosing the sampling distribution such that the integrand is constant minimizes the variance of the integral. The ideal sampling distribution should therefore be proportional to the numerator

$$\begin{aligned} q(x_{\text{part}}|x_{\text{reco}}) &\propto p_\theta(x_{\text{part}}) p(x_{\text{reco}}|x_{\text{part}}) \\ &\propto p_\theta(x_{\text{part}}|x_{\text{reco}}). \end{aligned} \quad (10)$$

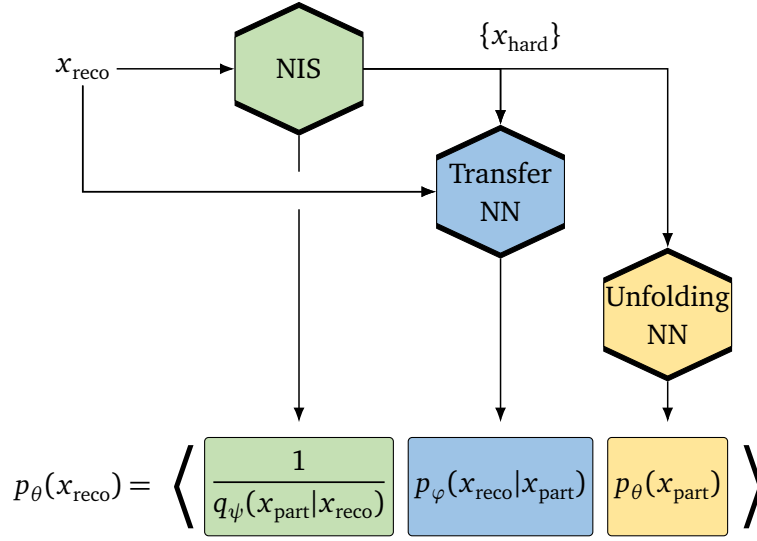


Figure 1: Reco-level maximum likelihood training of the unfolding network  $p_{\theta}(x_{\text{part}})$ .

In the second step we have applied Bayes' theorem to eliminate the direct dependence on  $p_{\theta}(x_{\text{part}})$ , but the conditional distribution,  $p_{\theta}(x_{\text{part}}|x_{\text{reco}})$  is still defined implicitly via  $p_{\theta}(x_{\text{part}})$  and  $p(x_{\text{reco}}|x_{\text{part}})$  and changes during the training of the unfolding network. For the NIS network we use the paired simulations  $(x_{\text{part}}, x_{\text{reco}})$  to train it on the inverse conditional distribution [9, 16]

$$q_{\psi}(x_{\text{part}}|x_{\text{reco}}) \approx p_{\text{sim}}(x_{\text{part}}|x_{\text{reco}}). \quad (11)$$

It is proportional to  $p_{\text{sim}}(x_{\text{part}})$  instead of  $p_{\theta}(x_{\text{part}})$ . Therefore, it will not give the ideal sampling distribution, but as long as  $p_{\theta}(x_{\text{part}})$  is not too far from its simulation counterpart, it will serve as an efficient importance sampling distribution. Unlike for generative unfolding, this conditional generative network serves as a numerical tool for training  $p_{\theta}(x_{\text{part}})$ . Any prior dependence will decrease the training efficiency, but not affect the unfolding result.

Combining Eq.(9) with neural importance sampling, the training of the forward unfolding of a single reco-level event now minimizes

$$\begin{aligned}
 \mathcal{L}_{\text{SPINUP}} &= - \int dx_{\text{reco}} p_{\text{data}}(x_{\text{reco}}) \log p_{\theta}(x_{\text{reco}}) \\
 &= - \int dx_{\text{reco}} p_{\text{data}}(x_{\text{reco}}) \log \int dx_{\text{part}} q_{\psi}(x_{\text{part}}|x_{\text{reco}}) \frac{p(x_{\text{reco}}|x_{\text{part}})p_{\theta}(x_{\text{part}})}{q_{\psi}(x_{\text{part}}|x_{\text{reco}})} \\
 &= - \lim_{N_{\text{MC}} \rightarrow \infty} \int dx_{\text{reco}} p_{\text{data}}(x_{\text{reco}}) \log \frac{1}{N_{\text{MC}}} \sum_{\{x_{\text{part}}\}} \frac{p(x_{\text{reco}}|x_{\text{part}})p_{\theta}(x_{\text{part}})}{q_{\psi}(x_{\text{part}}|x_{\text{reco}})} \Big|_{x_{\text{part}} \sim q_{\psi}(x_{\text{part}}|x_{\text{reco}})}.
 \end{aligned} \quad (12)$$

The training is illustrated in Fig. 1. The NIS network  $q_{\psi}(x_{\text{part}}|x_{\text{reco}})$  and the transfer network  $p_{\varphi}(x_{\text{reco}}|x_{\text{part}})$  are trained ahead of time, and their parameters are frozen during the main training of the unfolding network  $p_{\theta}(x_{\text{part}})$ .

**Pre-training** While NIS significantly eases its computational cost, the loss calculation in Eq.(12) remains a computational challenge, and convergence is slow. In Eq.(7) we have introduced a sum over  $N_{\text{MC}}$  samples to evaluate the  $x_{\text{part}}$ -integration. To speed up convergence, we pre-train the unfolding network on a single part-level event, i.e.  $N_{\text{MC}} = 1$ . The sum within the

logarithm is then reduced to a single summand and the calculation of the gradient simplifies substantially

$$\begin{aligned} \mathcal{L}_{\text{Pre}} &= - \int dx_{\text{reco}} p_{\text{data}}(x_{\text{reco}}) \log \frac{p(x_{\text{reco}}|x_{\text{part}})p_{\theta}(x_{\text{part}})}{q_{\psi}(x_{\text{part}}|x_{\text{reco}})} \Bigg|_{x_{\text{part}} \sim q_{\psi}(x_{\text{part}}|x_{\text{reco}})} \\ \Rightarrow \nabla_{\theta} \mathcal{L}_{\text{Pre}} &= - \int dx_{\text{reco}} p_{\text{data}}(x_{\text{reco}}) \nabla_{\theta} \log p_{\theta}(x_{\text{part}}) \Bigg|_{x_{\text{part}} \sim q_{\psi}(x_{\text{part}}|x_{\text{reco}})}. \end{aligned} \quad (13)$$

For the gradient of the pre-training loss, the two conditional probabilities do not contribute. The setup reduces to the likelihood training of  $p_{\theta}(x_{\text{part}})$  on the part-level distribution obtained by unfolding  $p_{\text{data}}(x_{\text{reco}})$  with  $q_{\psi}(x_{\text{part}}|x_{\text{reco}})$ . After pre-training,  $p_{\theta}(x_{\text{part}})$  corresponds to the outcome of generative unfolding acting on  $p_{\text{data}}(x_{\text{reco}})$ , including a potential prior dependence. For SPINUP it serves as a network initialization only. To validate the prior independence given numerical limitations of network trainings we have cross-checked that the pre-training only impacts the convergence time and not the result itself.

**Categorical approximation** To further improve the ML-computation of the loss we employ another approximation [50]. The log-likelihood for one reco-event in Eq.(12) reads

$$\mathcal{L}_{\text{SPINUP}} \approx \log \frac{1}{N_{\text{MC}}} \sum_i^{N_{\text{MC}}} w_i \quad \text{with} \quad w_i = \frac{p(x_{\text{reco}}|x_{\text{part}}) p_{\theta}(x_{\text{part}})}{q_{\psi}(x_{\text{part}}|x_{\text{reco}})} \Bigg|_{x_{\text{part}} \sim q_{\psi}(x_{\text{part}}|x_{\text{reco}})} \quad (14)$$

We can rewrite its gradient as

$$\nabla_{\theta} \mathcal{L}_{\text{SPINUP}} \approx \frac{1}{\sum_i^{N_{\text{MC}}} w_i} \sum_i^{N_{\text{MC}}} \nabla_{\theta} w_i = \sum_i^{N_{\text{MC}}} \frac{w_i}{\sum_i^{N_{\text{MC}}} w_i} \nabla_{\theta} \log w_i \quad (15)$$

The gradient  $\nabla_{\theta} \log p_{\theta}$  is given by the expectation value of  $\nabla_{\theta} \log w_i$  under a discrete categorical distribution with  $N_{\text{MC}}$  classes with class probabilities  $w_i / \sum_i^{N_{\text{MC}}} w_i$ . We can approximate it with a single draw from the distribution as

$$\nabla_{\theta} \mathcal{L}_{\text{SPINUP}} \approx \nabla_{\theta} \log w_i \quad \text{with} \quad w_i \sim \mathcal{C} \left( \frac{w_1}{\bar{w}}, \dots, \frac{w_{\text{MC}}}{\bar{w}} \right) \quad (16)$$

For this unbiased estimator of the original Monte Carlo estimator gradient we still draw  $N_{\text{MC}}$  samples from the importance sampling distribution to calculate the categorical weights in Eq.(16), but we only back-propagate gradients with respect to one of these samples. This approximation increases the estimator variance, but saves memory and in turn allows for a larger batch size or more Monte Carlo samples. We find this a favorable trade-off.

Finally, we achieve a speed-up through multiple backpropagation steps per batch, using the same categorical distribution. Since this does not require drawing new samples from the importance sampling network or re-evaluating the transfer density, it comes at very little additional cost.

**SPINUP** The above steps define an algorithm, where we assume access to paired simulated events at part- and reco-level as well as to data at reco-level.

1. Train the generative transfer network  $p_{\varphi}(x_{\text{reco}}|x_{\text{part}})$  on the paired simulated data;
2. Train the generative NIS network  $q_{\psi}(x_{\text{part}}|x_{\text{reco}})$  on the paired simulated data;
3. Pre-train the generative unfolding network  $p_{\theta}(x_{\text{part}})$  with  $N_{\text{MC}} = 1$  as an initialization;
4. Train the unfolding network  $p_{\theta}(x_{\text{part}})$  to reproduce the data, using the categorical approximation of the maximum likelihood loss, Eq.(12).

Notably, this will avoid a prior dependence without any iteration.

**Network architectures** SPINUP includes three separate generative networks, the transfer network  $p_\varphi(x_{\text{reco}}|x_{\text{part}}) \approx p(x_{\text{reco}}|x_{\text{part}})$ , the NIS network  $q_\psi(x_{\text{part}}|x_{\text{reco}}) \approx p_{\text{sim}}(x_{\text{part}}|x_{\text{reco}})$ , and the unfolding network  $p_\theta(x_{\text{part}})$ . Our choice of architectures is guided by the specific role played by these networks.

Diffusion networks are the state of the art in generative HEP applications [51], but they are not suitable for any of the networks in our setup due to their slow density evaluation. Here, normalizing flows are ideal, achieving comparable precision at an order of magnitude reduced computational cost [46].

For the transfer and unfolding networks, our loss calculation requires fast and precise density estimation, but does not require sample generation. We employ the Transfermer network [46], which has shown an excellent precision-speed trade-off in an application closely related to ours. It combines a Transformer backbone with one-dimensional RQS-splines, that autoregressively encode the density. The slow sampling coming with autoregressive generation does not matter for our application, since these networks are only used for density estimation.

The NIS network generates large numbers of samples in each training iteration. It requires an architecture for fast generation, potentially trading-off some precision. We employ an INN with RQS spline blocks [47–49].

**Ensembling** We employ ensembling for a rough estimate of the uncertainty introduced by our methodology. Typically, ensembling is used to estimate the uncertainty associated with the stochastic network initialization and training.

In our setup, it gives a lower bound on one additional source of uncertainty, the loss of information in the forward mapping. Since the loss calculation happens purely at the reco-level, any unfolded distribution  $p_\theta(x_{\text{part}})$  which reproduces the observed data minimizes the loss. If the ensemble is well-trained, every network will reproduce the same reco-level distribution, while mapping out a space of possible solutions at part-level. Such an ensemble comes with no guarantee to find every possible part-level solution, so the ensemble uncertainty should be viewed as a lower bound on the true information loss uncertainty.

### 3 Gaussian illustration

An instructive example for forward unfolding is a Gaussian toy model. We assume that the simulated and target distributions are normal distributions,

$$\begin{aligned} p_{\text{sim}}(x_{\text{part}}) &= \mathcal{N}(x_{\text{part}}; 0, 1) \\ p_{\text{truth}}(x_{\text{part}}) &= \mathcal{N}(x_{\text{part}}; 0.2, 0.9). \end{aligned} \quad (17)$$

The difference represents a small discrepancy between simulation and truth. Also the detector effects are assumed to be a simple Gaussian smearing,

$$p(x_{\text{reco}}|x_{\text{part}}) = \mathcal{N}(x_{\text{reco}}; x_{\text{part}}, \sigma_{\text{smear}}). \quad (18)$$

We can then calculate the reco-level distributions as

$$\begin{aligned} p_{\text{sim}}(x_{\text{reco}}) &= \int dx_{\text{part}} p_{\text{sim}}(x_{\text{part}}) p(x_{\text{reco}}|x_{\text{part}}) = \mathcal{N}(x_{\text{reco}}; 0, \sqrt{1 + \sigma_{\text{smear}}^2}) \\ p_{\text{data}}(x_{\text{reco}}) &= \int dx_{\text{part}} p_{\text{truth}}(x_{\text{part}}) p(x_{\text{reco}}|x_{\text{part}}) = \mathcal{N}(x_{\text{reco}}; 0.2, \sqrt{0.9^2 + \sigma_{\text{smear}}^2}). \end{aligned} \quad (19)$$

During unfolding we observe the two reco-level distributions in Eq.(19) and know the transfer function Eq.(18) from simulated paired events. The task is to infer  $p_{\text{truth}}(x_{\text{part}})$ , with the known outcome

$$\sigma_{\text{truth}}^2 = \sigma_{\text{data}}^2 - \sigma_{\text{smear}}^2. \quad (20)$$

The part-level distributions Eq.(17) and the corresponding reco-level distributions Eq.(19) for  $\sigma_{\text{smear}} = 1$  and 3 are shown in the left panels of Fig. 2. At part-level there is a clear difference between the simulated and truth distributions. For a precise detector with  $\sigma_{\text{smear}} = 1$  the two distributions are still clearly separated at reco-level. For  $\sigma_{\text{smear}} = 3$ , the two reco-level distributions are hard to distinguish, implying that reconstructing the truth will be difficult.

In the center and the right column of Fig. 2 we show unfolding results from an ensemble of 32 networks. The upper row shows the unfolded, part-level distributions, the lower row the corresponding reco-level distributions after convoluting with the forward simulation. For both smearing strengths, the ensemble of reco-level solutions matches the observed data without a significant spread. This implies that the unfolded distributions are valid. At part-level we see a large difference between the ensemble spreads for the two smearing strengths. Ensembles come with no guarantee to map out the space of possible solutions, so these uncertainties should be taken with caution, but they confirm that a large loss of information in the forward simulation causes a large uncertainty on the unfolded distribution.

To see that the algorithm has solved its task, we fit Gaussians to the SPINUP solutions at both reco- and part-level. For the widths we find

$$\begin{aligned} \sigma_{\text{smear}} = 1 : \quad & \sigma_{\text{reco}}^2 = 1.813 \pm 0.0169 \text{ (truth 1.81)} \quad \sigma_{\text{part}}^2 = 0.814 \pm 0.0166 \text{ (truth 0.81)} \\ \sigma_{\text{smear}} = 3 : \quad & \sigma_{\text{reco}}^2 = 9.853 \pm 0.095 \text{ (truth 9.81)} \quad \sigma_{\text{part}}^2 = 0.859 \pm 0.091 \text{ (truth 0.81)}. \end{aligned}$$

At reco-level, for both smearing strengths SPINUP recovers the correct squared width with a relative precision of roughly 1 percent. Applying Gaussian error propagation to Eq. 20 yields

$$\Delta\sigma_{\text{truth}}^2 + \Delta\sigma_{\text{smear}}^2 = \Delta\sigma_{\text{data}}^2. \quad (21)$$

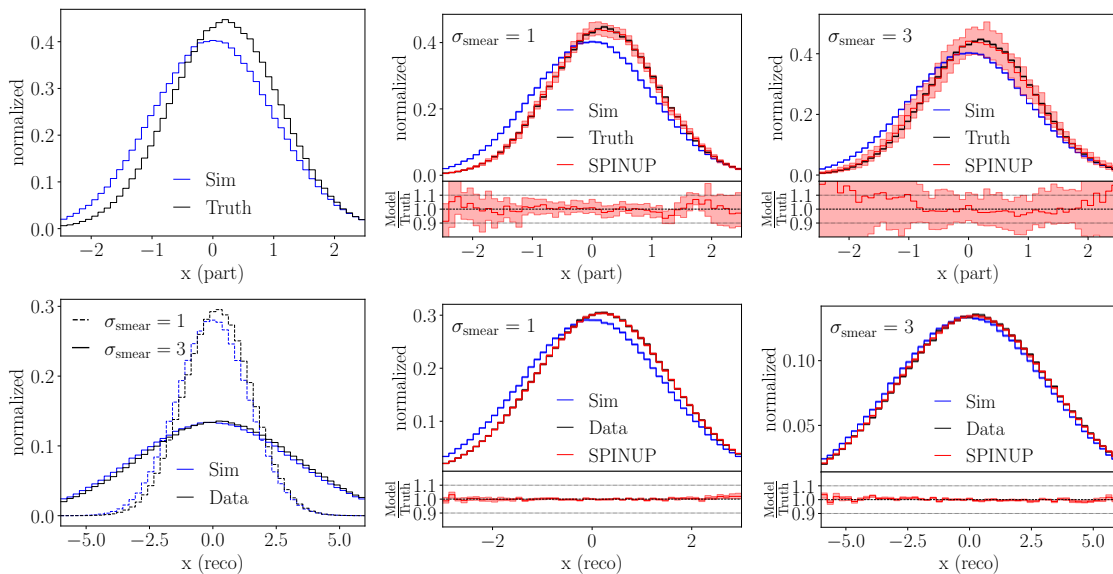


Figure 2: Unfolding results for the Gaussian toy for  $\sigma_{\text{smear}} = 1, 3$ . The upper row shows the part-level unfolded distributions, the lower row the obtained reco-level distributions. Uncertainties are obtained from an ensemble of 32 networks.

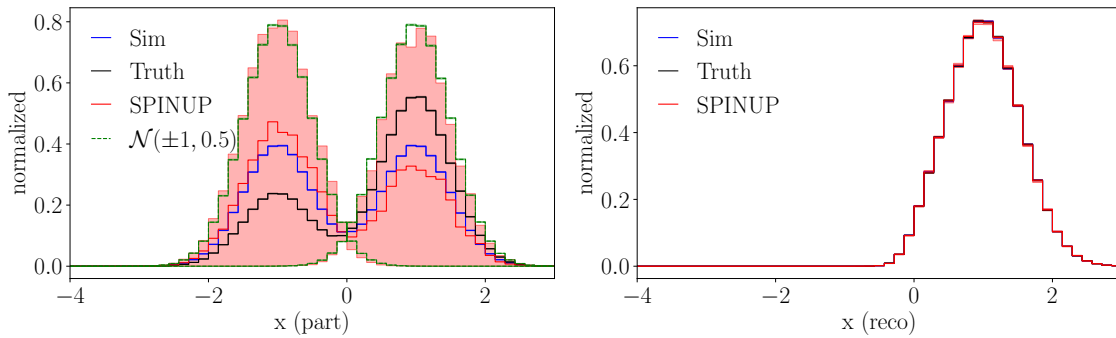


Figure 3: Part-level and reco-level distributions for the sign loss toy example Eqs.(22) and (23). Unfolding results are shown for an ensemble of 32 networks.

Assuming no error on the smearing widths, the absolute error on the squared widths at reco- and at part-level should be the same. We observe this to be the case for the SPINUP uncertainties. Since the reco-level widths are significantly larger than the part-level width, this propagation of the absolute value of the uncertainties results in a larger relative uncertainty at part-level. For the  $\sigma_{\text{smear}} = 1$  case we observe a relative uncertainty of roughly 2 percent at part-level, while for the  $\sigma_{\text{smear}} = 3$  case the relative uncertainty is about 10 percent.

**Information loss** For a drastic information loss we consider a mixture of two Gaussians,

$$p(x_{\text{part}}|\alpha) = \alpha \mathcal{N}(x_{\text{part}}; -1, 0.5) + (1 - \alpha) \mathcal{N}(x_{\text{part}}; 1, 0.5) \\ \text{with } \alpha_{\text{sim}} = 0.5 \quad \alpha_{\text{truth}} = 0.3 . \quad (22)$$

We consider a forward mapping that loses the sign and adds Gaussian smearing,

$$x_{\text{reco}} = |x_{\text{part}}| + \mathcal{N}(0, 0.2) . \quad (23)$$

By construction, every  $\alpha$  will lead to the same reco-level distribution.

The toy dataset and the SPINUP unfolding results are shown in Fig. 3. The left panel shows the part-level distributions, the right panel the corresponding reco-level distributions after convoluting with the forward simulation. At part-level, the ensemble of 32 networks shows a huge spread, indicating a wide range of valid solutions. It turns out that the ensemble does map out the entire solution space. This is showcased by the two green curves, the boundary cases  $\mathcal{N}(\pm 1, 0.5)$  for  $\alpha = 0, 1$ . The right plot confirms that all of these part-level solutions collapse to the identical observed distribution at reco-level.

## 4 Jet substructure dataset

As a physics toy example we look at the OmniFold dataset [8], a simple benchmark for unfolding tools [13, 15, 17, 23, 52]. It consists of 1.6M simulated LHC events for the process

$$pp \rightarrow Z + \text{jets} \quad (24)$$

at 14 TeV. To emulate the difference between Monte Carlo simulation and data, we use two versions: first, events are generated with Pythia 8.244 [53] and Tune 26; second, events are generated with Herwig 7.1.5 [54] and standard tune. Both datasets use Delphes 3.5.0 [55] with the CMS card with particle-flow for the detector simulation. Jets are clustered before and

after Delphes using the anti- $k_T$  algorithm [56] with  $R = 0.4$ , implemented in FastJet 3.3.2 [57]. We consider the Herwig events at reco-level as data. The corresponding Herwig part-level events represent the unknown truth. The paired Pythia events serve as the simulation dataset,

$$p_\varphi(x_{\text{reco}}|x_{\text{part}}) \approx p_{\text{Pythia}}(x_{\text{reco}}|x_{\text{part}}). \quad (25)$$

The goal is to unfold jet substructure measurements. The six observables used are the jet mass, width, multiplicity, soft drop mass [58, 59], momentum fraction, and the  $N$ -subjettiness ratio [60],

$$\left\{ m, \tau_1^{(\beta=1)}, N, \rho = \frac{m_{\text{SD}}^2}{p_T^2} z_g, \tau_{21} = \frac{\tau_2^{(\beta=1)}}{\tau_1^{(\beta=1)}} \right\} \quad (26)$$

with  $z_{\text{cut}} = 0.1$  and  $\beta = 0$  for the momentum fraction.

We train SPINUP on this 6-dimensional phase space. The transfer and NIS networks are pre-trained on the Pythia event pairs. The unfolding training uses the Herwig reco-level events. The unfolded jet mass distribution is shown in the left panel of Fig. 4. We see that SPINUP does not recover the correct truth, with deviations up to 10%.

To identify the underlying issue, we push the unfolded events through the learned transfer function and look at the reco-level distribution in the center panel of Fig. 4. We observe perfect closure, so with the given forward simulation SPINUP has fulfilled this task perfectly.

It could be that the solution space is degenerate, so SPINUP finds an unfolded distribution different from the (Herwig) truth, but still compatible with the data. However, in this particular dataset the problem is the forward simulation, as shown in the right panel of Fig. 4. It shows the distribution we find when applying the trained forward surrogate  $p_\varphi(x_{\text{reco}}|x_{\text{part}})$  to the Pythia and Herwig part-level datasets. For Pythia, it reproduces the reco-level distribution at the percent-level, but for Herwig we observe a significant discrepancy. This means the forward conditional probability does not generalize, violating a fundamental assumption of all unfolding algorithms.

**Forward simulation** The reason that the forward simulation does not generalize is the high-level summary statistics. In both datasets the detector effects are simulated with the same Delphes tune, so in the full low-level phase space the four-momenta of all individual particles are consistent between Pythia and Herwig. Once we look at jet observables, the loss of information induces a prior dependence in the forward simulation.

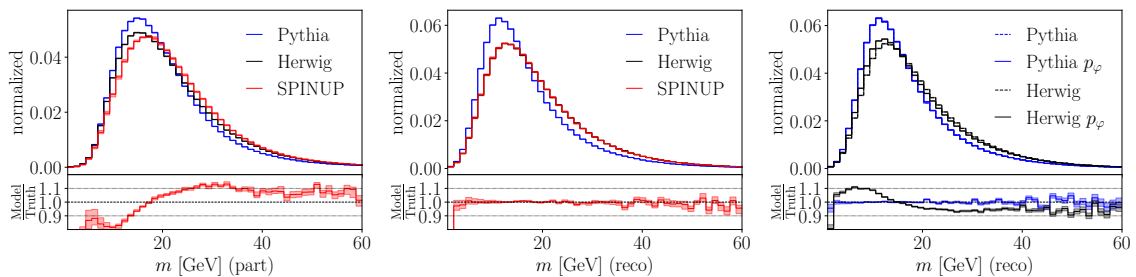


Figure 4: Left: part-level unfolding result for the jet mass. Center: reco-level distribution after passing the unfolding through the forward simulation. Right: transfer network  $p_\varphi(x_{\text{reco}}|x_{\text{part}})$  trained on Pythia and evaluated on both Pythia and Herwig. The full set of observables is shown in Figs. 13 and 14 in the Appendix.

This effect of a lossy summary statistics  $s_{\text{part}}(x_{\text{part}})$  can be seen by including it as an explicit condition in the forward simulation

$$p(x_{\text{reco}}|s_{\text{part}}) = \int dx_{\text{part}} p(x_{\text{reco}}|x_{\text{part}}) p(x_{\text{part}}|s_{\text{part}}). \quad (27)$$

The conditional probability  $p(x_{\text{reco}}|x_{\text{part}})$  is the complete forward mapping, while  $p(x_{\text{part}}|s_{\text{part}})$  inverts the computation of the summary statistics,

$$p(x_{\text{part}}|s_{\text{part}}) = p(s_{\text{part}}|x_{\text{part}}) \frac{p(x_{\text{part}})}{p(s_{\text{part}})}. \quad (28)$$

In case of information loss,  $p(s_{\text{part}}|x_{\text{part}})$  is well-defined, while the inverse includes degeneracies or flat directions. Without loss of information, this relation reduces to a change of variables. The prior dependence on  $p(x_{\text{part}})$  implies

$$\begin{aligned} p_{\text{Pythia}}(x_{\text{part}}|s_{\text{part}}) &\neq p_{\text{Herwig}}(x_{\text{part}}|s_{\text{part}}) \\ \Rightarrow p_{\text{Pythia}}(x_{\text{reco}}|s_{\text{part}}) &\neq p_{\text{Herwig}}(x_{\text{reco}}|s_{\text{part}}). \end{aligned} \quad (29)$$

This shortcoming could be addressed by unfolding the full phase space, leading to the challenge of scaling generative networks to  $\mathcal{O}(100)$  particles. To stick to our established benchmark, we instead circumvent this issue with a slight change to the dataset: instead of using the reco-level Herwig data, we use the trained 6-dimensional forward surrogate  $p_{\varphi}(x_{\text{reco}}|x_{\text{part}}) \approx p_{\text{Pythia}}(x_{\text{reco}}|x_{\text{part}})$  to generate synthetic reco-level jet substructure observables for the Herwig sample. This way, the forward simulation generalizes.

The consistent SPINUP results are shown in Fig. 5. Again, we train an ensemble of 32 unfolding networks and show the median together with the centered 68% range. We recover the correct Herwig part-level distributions over the entire phase space at the per-cent level. For most observables, the fluctuations are covered by the ensemble.

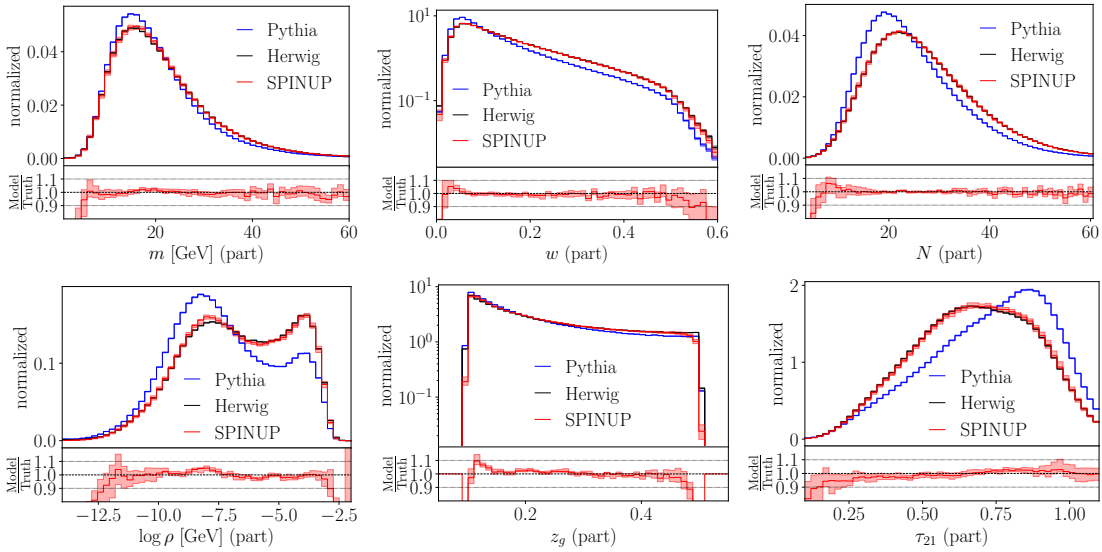


Figure 5: Part-level unfolded distributions from the fake Herwig reco-distribution.

## 5 Unfolding to parton level

As a proper test of SPINUP we include an unfolding application to parton level. An established, challenging example process is associated single-top and Higgs production with a purely hadronic signal [45, 46],

$$pp \rightarrow tHj \rightarrow (bjj)(\gamma\gamma)j + \text{jets}, \quad (30)$$

We allow for a complex top Yukawa coupling [61] with a CP-phase  $\alpha$ ,

$$\mathcal{L}_{t\bar{t}H} = -\frac{Y_t}{\sqrt{2}} \left[ a \cos \alpha (\bar{t}t) + ib \sin \alpha (\bar{t}\gamma_5 t) \right] H, \quad (31)$$

with  $a = 1$  and  $b = 2/3$  [62], keeping the cross section for  $gg \rightarrow H$  constant.

We define the parton level as the top, Higgs and forward jet before decays and QCD radiation, defining seven independent phase space dimensions. From there we apply the usual simulation chain with decays, parton shower and detector simulation, as described in Ref. [45]. At reco-level, we consider the momenta of the two photons, one b-tagged jet and the three light jets with the largest transverse momentum. We make a range of kinematic cuts, following Ref. [45].

The model dependence of the simulation is defined by the choice of  $\alpha$ . The parton-level momenta contain the complete information of the forward process, resulting in a model-independent transfer function. Looking at the parton-level distributions for  $\alpha = 0^\circ, 45^\circ, 90^\circ$  in Fig. 6, we observe that the angular separations are particularly sensitive. To ensure a good coverage of phase space for different CP-angles during the training of our transfer function, we generate 4.5M events with  $\alpha$  sampled uniformly between  $-180^\circ$  and  $180^\circ$ . For the training of the unfolding network we use 450K ‘measured’ reco-level events with  $\alpha = 45^\circ$ . The goal is to unfold to the parton level such that  $\alpha$  can be measured there without any training bias.

**Transfer function** We first look at the trained transfer function to confirm that  $p(x_{\text{reco}}|x_{\text{part}})$  generalizes between different  $\alpha$  values. As mentioned above, the training data is sampled uniformly between  $-180^\circ$  and  $+180^\circ$ , without conditioning. The hyperparameters can be found

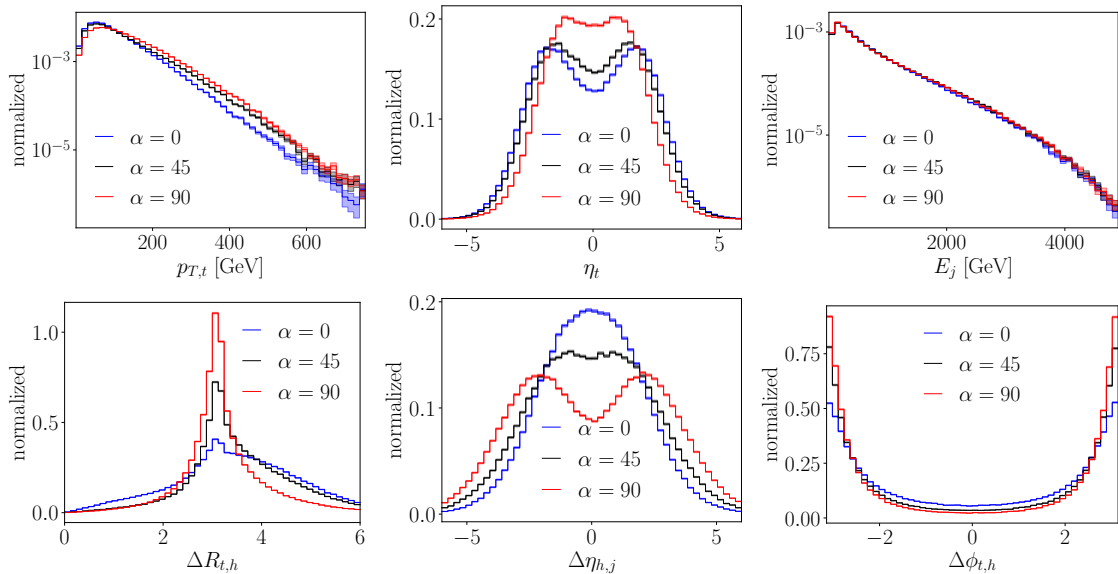


Figure 6: Dependence of the parton-level distribution on the parameter  $\alpha$

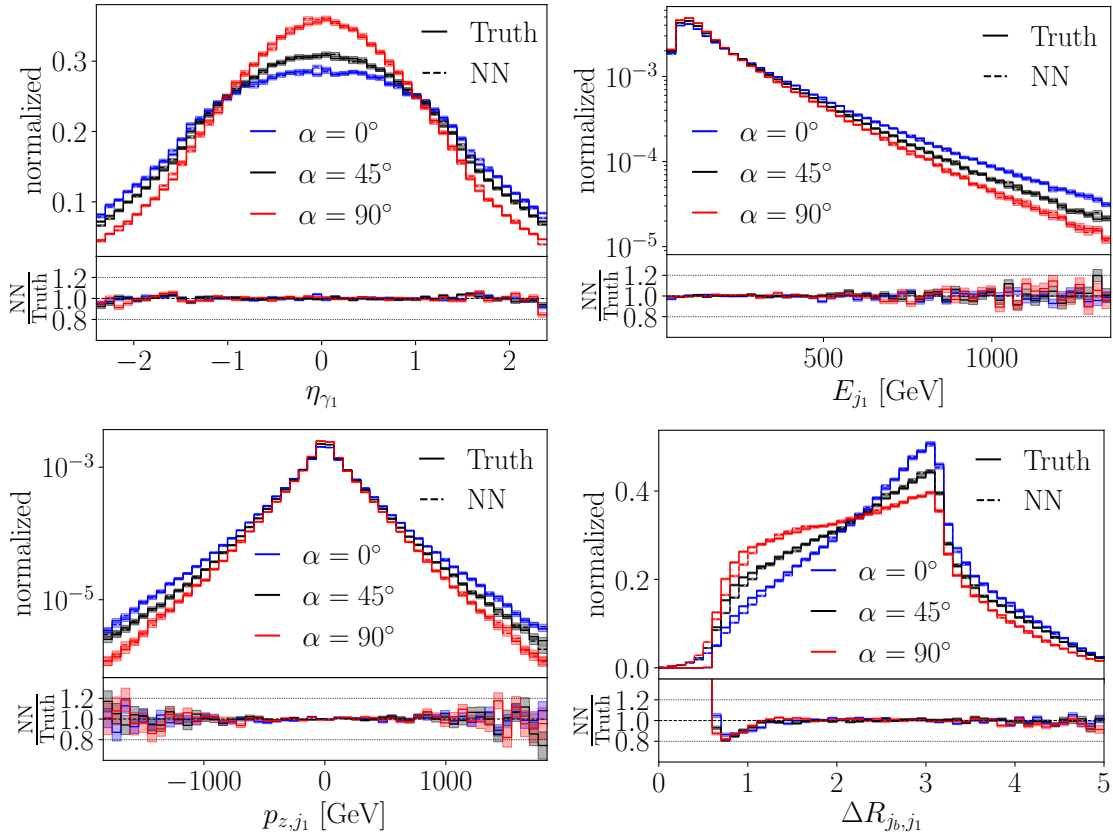


Figure 7: Transfer network trained on the  $tHj$  parton-level dataset

in Tab. 2 in the appendix. In Fig. 7 we show a set of reco-level distributions when applying the transfer network to parton-level distributions with  $\alpha = 0^\circ, 45^\circ, 90^\circ$ . In all cases the correct reco-level distributions are recovered, indicating no prior dependence in the forward mapping. In the  $\Delta R_{j_b, j_1}$  distribution the network interpolates through the jet algorithm cut at  $\Delta R_{j_b, j_1} = 0.4$ . Such a shortcoming in the learned transfer probability will inherently limit the precision of the unfolding. However, in our case it only affects a sub-leading feature, and we do not observe any general problems.

## 5.1 Unfolding

We illustrate the SPINUP performance for  $\alpha = 45^\circ$ . Again, we train an ensemble of networks and show the median and 68% quantiles. The training hyperparameters can be found in the appendix in Tab. 2. Some unfolded distributions at parton level are shown in Fig. 8. Deviations between truth and the unfolded distribution are at the percent-level over most of the phase space. It shows no sign of prior dependence and recovers the parton-level distribution for  $\alpha = 45^\circ$ . The observed reco-level distributions contain enough information to reconstruct the correct parton-level distribution and the method delivers this task.

The variation over the ensemble is very small over most of phase space and only mildly grow towards the tails, indicating that the method does not find significant degeneracy in the solution space. Notably, in  $E_j$  the tail towards large energies is consistently underestimated by all ensemble members.

We move on to the results at reco-level, obtained by passing the learned SPINUP unfolding through the forward network. Results for  $\alpha = 45^\circ$  are shown in Fig. 9. Reproducing the

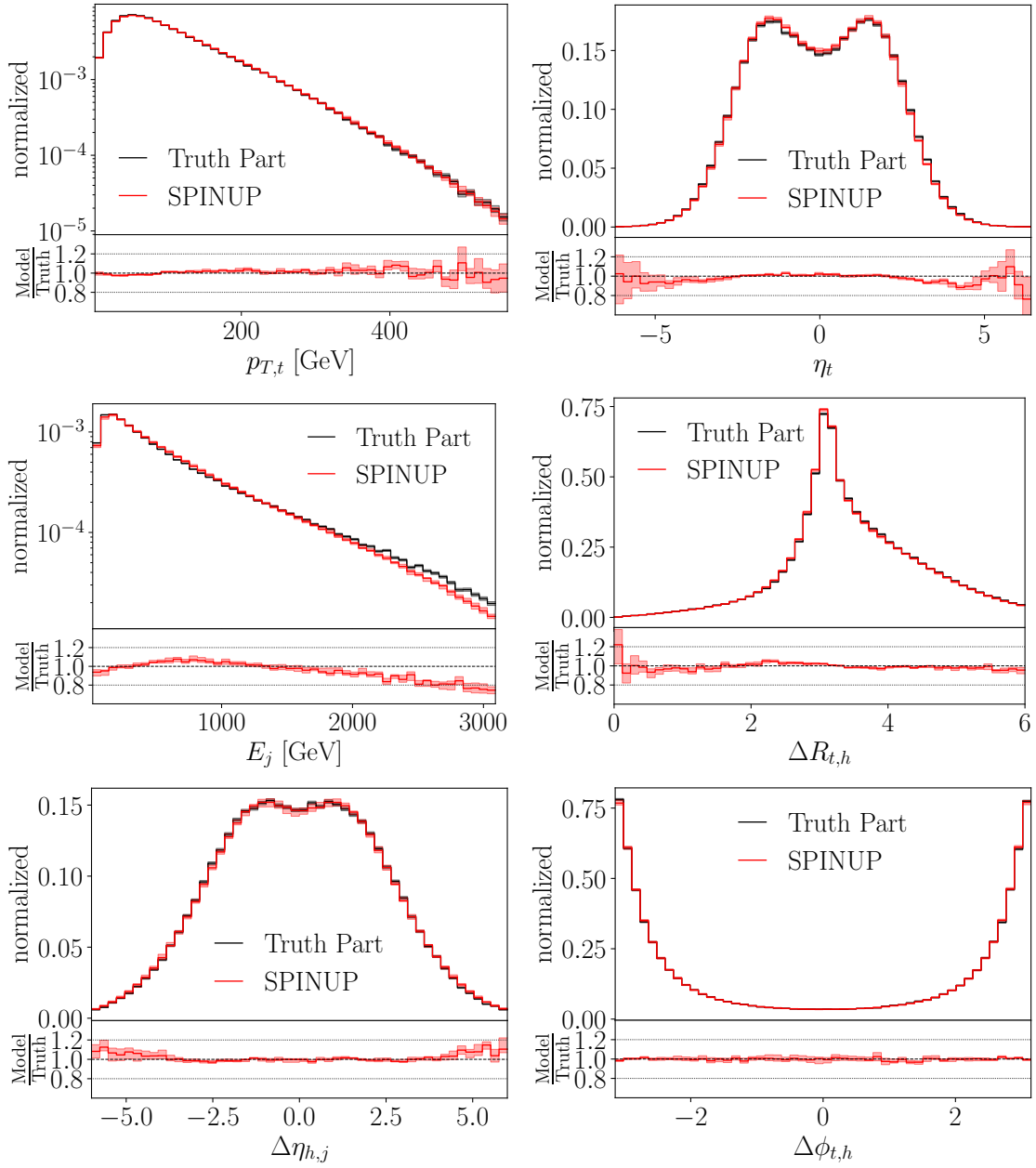


Figure 8: Unfolded observables at parton-level using SPINUP for  $\alpha = 45^\circ$ .

observed reco-level data is the training objective of the unfolding network. SPINUP faithfully reproduces the reco-kinematics with high precision, keeping differences between truth and unfolded distribution at the percent-level over the entire phase space. Again, our method does not show any signs of prior dependence. We observe reco-level data for a specific choice of  $\alpha$  and the method is trained to reproduce this observed distribution. In the  $\Delta R$  observables the mis-modelling at  $\Delta R = 0.4$  remains, because like any other density estimation neural network, SPINUP struggles to model hard cuts.

## 5.2 Inference

After demonstrating that SPINUP unfolds to partons at the per-cent level and without prior dependence, we test whether we can measure  $\alpha$  from unfolded, public data. At parton level

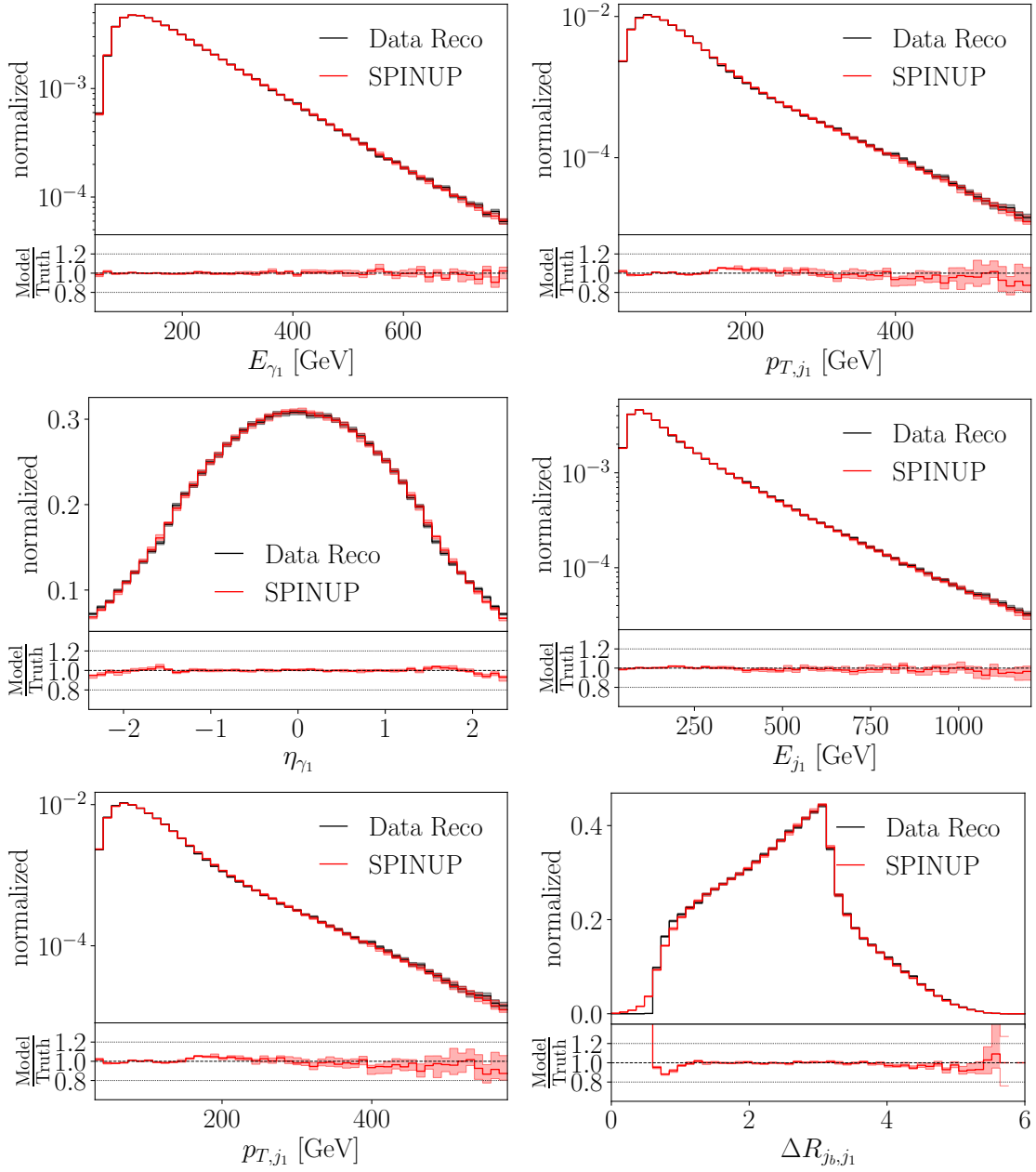


Figure 9: Reco-level observables for  $\alpha = 45^\circ$ , obtained by passing the SPINUP unfolding results through the forward model.

we have direct analytic access to the likelihood via the differential cross section

$$p(x_{\text{part}}|\alpha) = \frac{1}{\sigma(\alpha)} \frac{d\sigma(\alpha)}{dx_{\text{part}}}. \quad (32)$$

This means that we can evaluate the theory likelihood of an event under a parameter hypothesis  $\alpha$ . For a sample of parton level events  $\{x_{\text{part}, i}\}$ , we can calculate [63]

$$\mathcal{L}(\alpha) = \sum_i^{N_{\text{data}}} \log p(x_{\text{part}, i}|\alpha) \quad (33)$$

After unfolding, this inference step is technically trivial. We evaluate the likelihood on a fine grid of  $\alpha$  values and extract the maximum.

**Acceptance effects** One subtlety that we have to account for when using the differential cross section as in Eq.(32) is event acceptance. We apply an event selection at reco-level, which in turn leads to a smeared selection at parton-level. This is encoded in the efficiency  $\epsilon(x_{\text{part}})$ , defined as the probability to accept a given part-level event after forward simulation. All components of SPINUP are trained on the fiducial phase space after cuts, corresponding to the total cross section

$$\sigma_{\text{fid}}(\alpha) = \sigma(\alpha) \int dx_{\text{part}} \epsilon(x_{\text{part}}) p(x_{\text{part}}|\alpha). \quad (34)$$

This changes the learned or unfolded density over parton-level phase space to

$$p(x_{\text{part}}|\alpha) = \frac{1}{\sigma_{\text{fid}}(\alpha)} \frac{d\sigma(\alpha)}{dx_{\text{part}}} \epsilon(x_{\text{part}}), \quad (35)$$

This effect is discussed in detail in Ref. [46]. Following the same strategy we train a binary classifier  $\epsilon_{\theta}(x_{\text{part}})$  which predicts reco-level acceptance as a function of the parton-level kinematics. It will directly give us the acceptance probability and allow us to correct the densities.

**Results** To measure the CP-phase  $\alpha$  from unfolded data, we generate samples from the learned unfolding network  $x_{\text{part}} \sim p_{\text{unfold}}(x_{\text{part}})$  and calculate the parton-level log-likelihood on a grid of 1000 values  $\alpha_{\text{true}} \pm 15$ . We then extract the maximum-likelihood solution as the minimum of the resulting likelihood parabolas. We estimate the uncertainty by repeating this procedure 20 times.

The resulting error on  $\alpha$  scales with the number of sampled events. Since we have encoded the unfolded distribution in an unconditional generative network  $p_{\theta}(x_{\text{part}})$ , we can generate an arbitrary number of samples. Doing this with a single neural network sends the estimator uncertainty to zero. This is because this uncertainty only represents the MC approximation uncertainty of sampling a generative model rather than evaluating an explicit density. Instead, we have to take into account the uncertainty on the unfolded distribution itself, which is addressed by incorporating the spread from the trained ensemble. Instead of resampling the same network 20 times, we draw one sample of events from each of the 20 ensemble members. This gives us 20 estimates for  $\alpha$ .

The results from this procedure are shown in Fig. 10. The left panel shows the estimated  $\alpha$  using either 20 generated events sampled from a single network, or one event sample from each of the 20 networks in the full ensemble. The right panel shows the scaling of the uncertainty with the number of sampled events. Indeed, the unfolded distribution gives a correct measurement of  $\alpha$ , confirming that our SPINUP method has recovered the truth distribution.

Even using only 400 events from the sampled unfolded distribution,  $\alpha$  can already be estimated, albeit with a large uncertainty. In the low event number regime, the single network measurement and the ensemble measurement have similar uncertainties, indicating that they are dominated by the statistical fluctuations. When we increase the number of sampled events, the uncertainties decrease and the difference between the ensemble and the single network becomes visible. For the single network the uncertainties vanish, and no longer cover the true value for more than  $10^5$  samples. For the ensemble measurement the uncertainties reach a plateau when the statistical uncertainties on the individual estimates become negligible and we are dominated by the ensemble uncertainty. The ensemble translates the statistical uncertainty

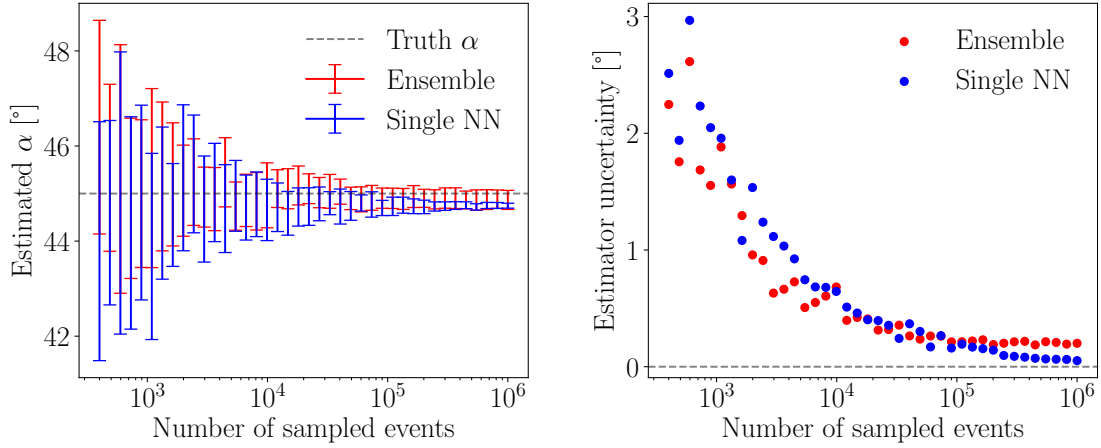


Figure 10: Parton-level parameter inference on the unfolded distribution for the  $\alpha = 45^\circ$  event sample. The uncertainties are the standard deviations over 20 event samples, either from the 20 different networks in the ensemble or from the same network repeatedly.

from a finite number of data events into a systematic uncertainty on the measured parameter, which covers the true value.

Alternatively, we can look at the log-likelihood parabolas extracted from 5 networks from the SPINUP ensemble shown in Fig. 11. The left panel shows parabolas calculated with 1K events sampled from the networks. They are scattered around the true  $\alpha = 45^\circ$ , but due to the small number of sampled events they are very broad and do not allow a precise measurement. The uncertainty is dominated by the statistical uncertainties of the individual estimates. For large statistics with 1M sampled events, shown in the right panel, the individual parabolas become very narrow and the uncertainty is dominated by the spread of the minima positions.

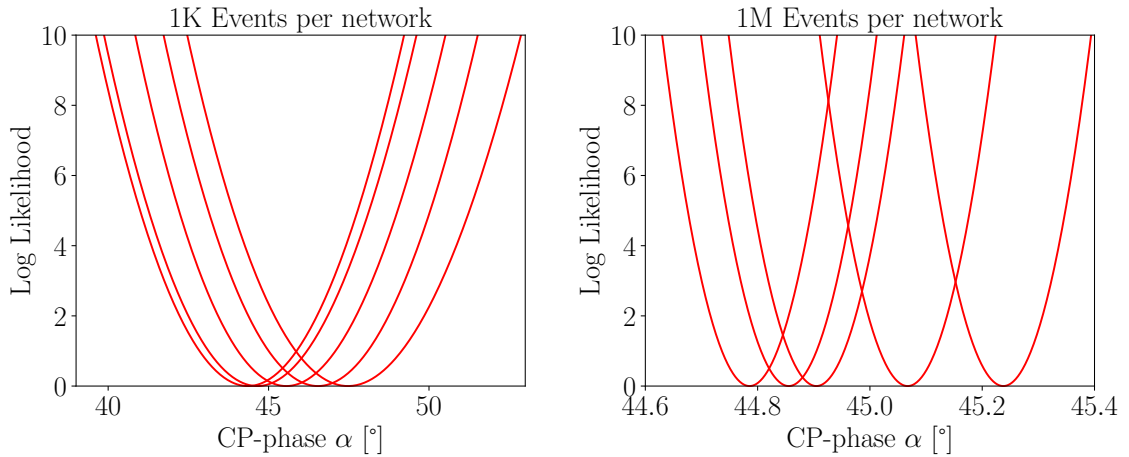


Figure 11: Likelihood parabolas from 5 networks from the SPINUP ensemble. The left plot shows results from 1K events sampled per network, the right plot shows results for sampling 1M events per network.

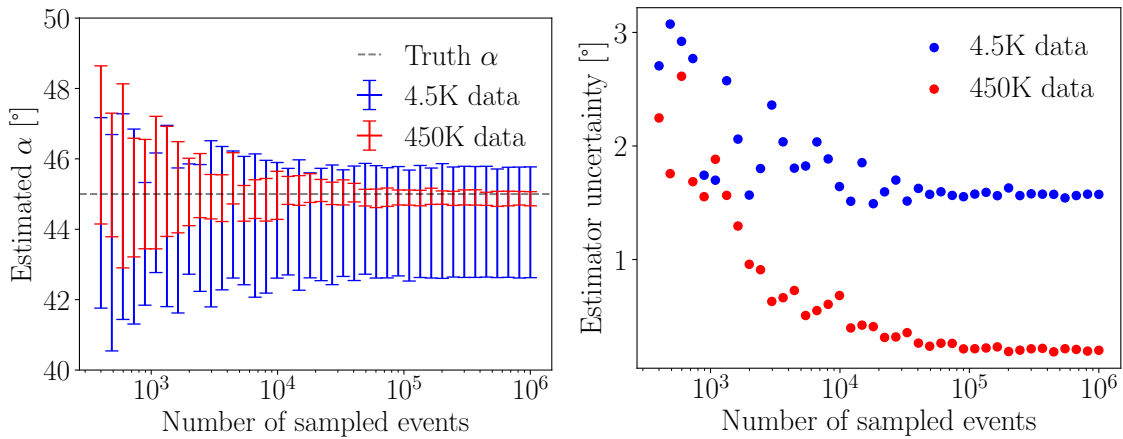


Figure 12: Parton-level parameter inference on the unfolded distribution for the  $\alpha = 45^\circ$  event sample. The uncertainties are derived from the network ensemble.

### 5.3 Lower data statistic

Finally, we investigate the behavior of SPINUP when training the algorithm on a lower number of measured reco-level events. We leave the number of simulated events used to train the transfer and NIS networks invariant. This allows us to emulate the realistic scenario of unfolding a process with a small fiducial cross section, such as  $tHj$ .

In Fig. 12 we compare the parameter estimation results from training SPINUP on either the full ‘measured’ dataset (450K events) or just 1 percent of that dataset (4.5K events). We observe that even for just 4.5K measured events, SPINUP allows to accurately recover the theory parameter from the unfolded distribution. The uncertainty in the parameter estimation is significantly larger, as we would expect.

If the ensembling uncertainty captured purely the statistical uncertainty from limited training data, we would expect it to scale as  $\frac{1}{\sqrt{n}}$ . However, the ensemble also captures other sources of uncertainty, such as stochastic network initialization and training, and potential degeneracy in the solution space. In this preliminary experiment we observe the factor to be almost  $\frac{1}{\sqrt{n}}$ , indicating that the limited statistics are the leading source of uncertainty. We leave a more systematic study of the uncertainties for future work.

## 6 Outlook

Modern machine learning makes it possible to precisely unfold high-dimensional, unbinned spaces, relying on reweighting, distribution mapping, or posterior estimation. SPINUP instead estimates the forward mapping and extracts the unfolded distribution by proposing part-level configurations with neural importance sampling. The forward information loss is captured with ensembling. Technically, SPINUP combines a forward transfer network, a NIS network, and the generative unfolding network.

We first illustrated SPINUP for Gaussian toy models, where it extracts the part-level truth, clearly separated from the part-level simulation used to train the transfer network. The reco-level data can be recovered with a convolution with the transfer network. This remains true even for a larger smearing where the reco-level for simulation and truth become very similar, and the ensembling captures the increased uncertainty of the unfolded part-level distribution.

In the example of a bimodal Gaussian distribution with a peak at positive and negative values, and a forward process that loses the sign information, we find that the ensemble maps out the space of possible part-level distributions that map to the same reco-level distributions, again confirming the effectiveness of our ensembling procedure.

Next, we apply our method to the OmniFold dataset [8], a widely used benchmark dataset for machine-learning based unfolding methods containing a set of six jet-substructure observables in Z+jets production. Using events generated by Pythia as simulation and events generated by Herwig as truth, we find that the unfolded distribution does not recover the truth, with deviations up to 10%. However, this is not due to a lack of precision of our unfolding method. Instead, the model-independence of the forward mapping is lost in the reduction of the high-dimensional space of jet-constituent four-momenta to jet-substructure observables, violating a fundamental assumption of unfolding. We demonstrate that our method is able to recover the truth distribution at the percent level for a synthetic reco-level dataset sampled using our learned transfer function.

Finally, we use SPINUP to unfold associated single-top and Higgs production events to parton level. We allow for mixed CP-even and CP-odd interactions in the top Yukawa coupling with a CP-phase  $\alpha$ . We train our transfer network on events with a uniformly distributed CP-phase and then unfold reco-level events with  $\alpha = 45^\circ$ , recovering most parton-level distributions with percent-level precision. We then use the analytic expression for the matrix element to extract a log-likelihood for  $\alpha$  from the unfolded data and correctly infer the parameter. We estimate the uncertainty arising from our unfolding procedure by repeating the inference for an ensemble of unfolding networks. Moreover, we show that the SPINUP method remains robust for very low numbers of measured events.

Altogether, the SPINUP method is a valuable addition to the growing selection of ML-based unfolding methods as it is simulation-prior independent by construction and is suitable even for applications with large losses of information in the forward process and low numbers of unfolded events.

## Acknowledgments

We thank Sofia Palacios Schweitzer for very fruitful discussions, and for simulating the top decay dataset. NH is supported by the BMBF Junior Group Generative Precision Networks for Particle Physics (DLR 01IS22079). MK is supported by the US Department of Energy (DOE) under grant DE-AC02-76SF00515. TH is supported by the PDR-Weave grant FNRS-DFG numéro T019324F (40020485). This work was supported by the DFG under grant 396021762 – TRR 257: *Particle Physics Phenomenology after the Higgs Discovery*, and through Germany's Excellence Strategy EXC 2181/1 – 390900948 (the *Heidelberg STRUCTURES Excellence Cluster*). The authors acknowledge support by the state of Baden-Württemberg through bwHPC and the German Research Foundation (DFG) through grant INST 35/1597-1 FUGG.

## A Hyperparameters

Parameter	Unfolding-NN	Transfer-NN	Sampling-NN
Network	Transfermer	Transfermer	INN
Optimizer	Adam	Adam	Adam
Learning rate	0.001	0.0003	0.0003
LR schedule	Cosine annealing	One cycle	One cycle
Batch size	512	1024	1024
Epochs	60	200	200
INN Blocks	-	-	6
Subnet layers	5	5	5
Subnet dim	256	256	256
RQS bins	20	20	20
Transformer blocks	4	4	-
Transformer heads	4	4	-
Embedding dim	64	64	-
Feedforward dim	256	256	-
MC samples	64	-	-
Pretrain epochs	200	-	-

Table 1: Network and training hyperparameters for the jet substructure dataset in Sec. 4

Parameter	Unfolding-NN	Transfer-NN	Sampling-NN
Network	Transfermer	Transfermer	INN
Optimizer	Adam	Adam	Adam
Learning rate	0.001	0.0003	0.0003
LR schedule	Cosine annealing	One cycle	One cycle
Batch size	512	1024	1024
Epochs	30	350	350
INN Blocks	-	-	20
Subnet layers	5	5	5
Subnet dim	256	256	256
RQS bins	30	30	30
Transformer blocks	6	6	-
Transformer heads	6	6	-
Embedding dim	64	64	-
Feedforward dim	256	256	-
MC samples	64	-	-
Pretrain epochs	50	-	-

Table 2: Network and training hyperparameters for the parton level  $tHj$  dataset in Sec. 5

## B Additional results

### Jet substructure dataset

#### Transfer model

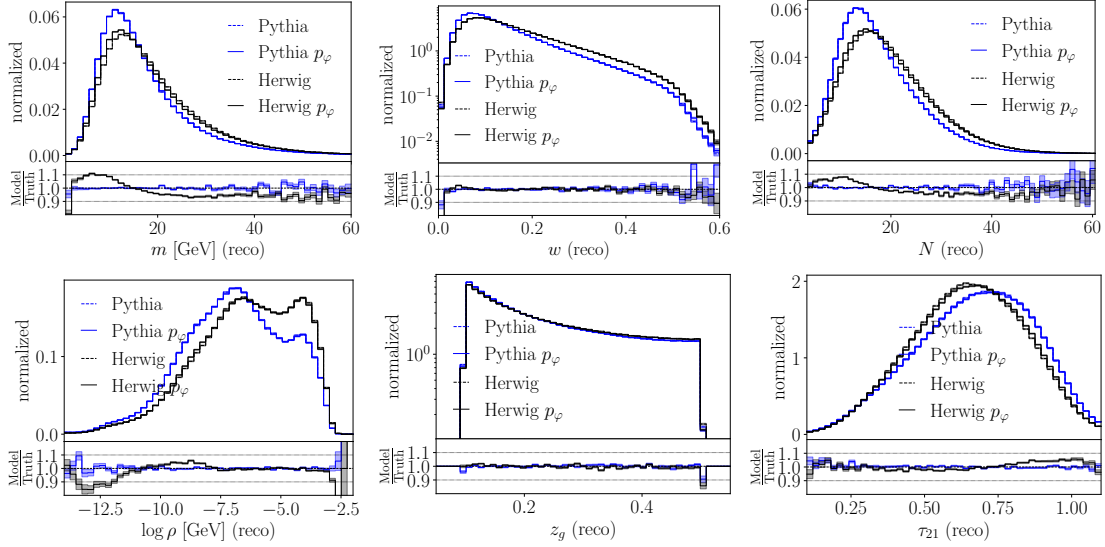


Figure 13: Full set of plots for the transfer model trained on Pythia and applied to Herwig.

#### Unfolding results on original Herwig

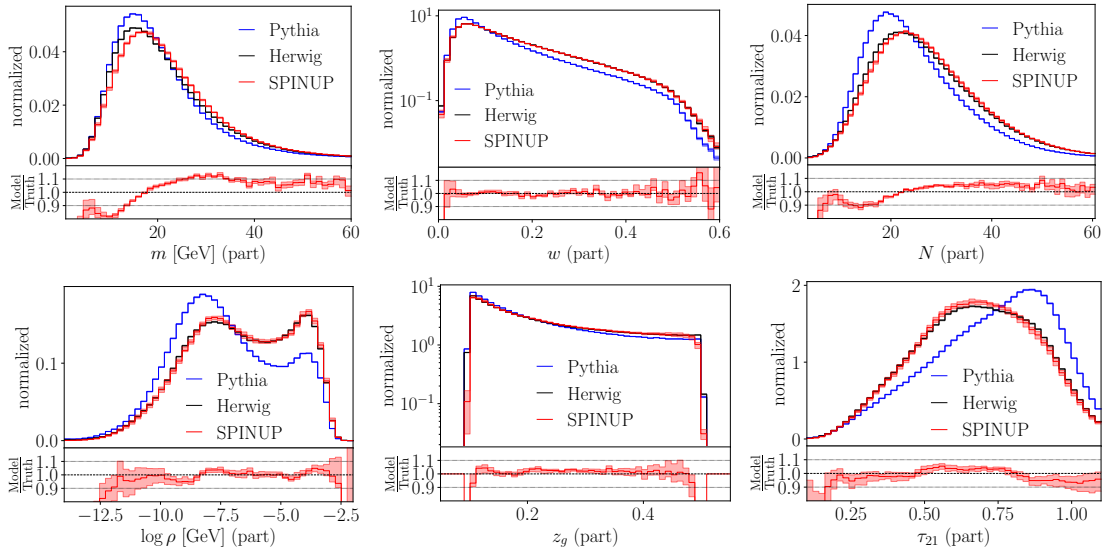


Figure 14: Part-level unfolded distributions obtained by running the method on the reco-level Herwig distribution.

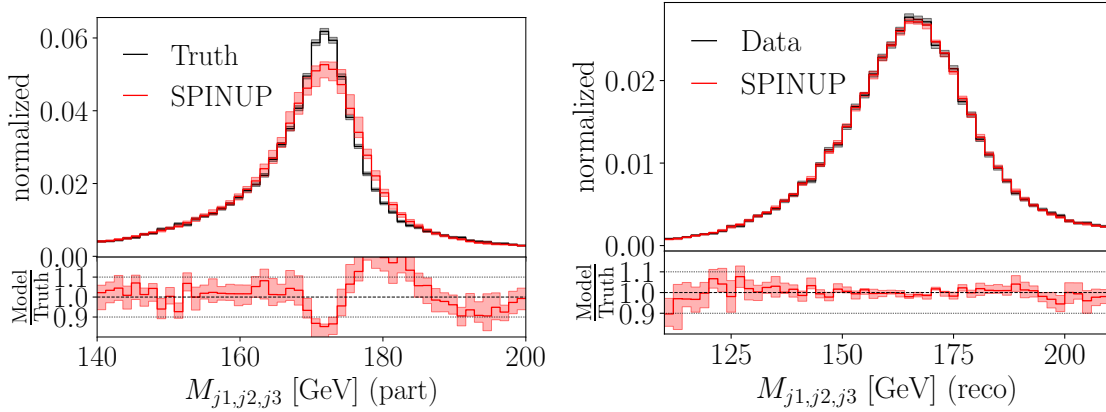


Figure 15: SPINUP results for the  $M_{j_1,j_2,j_3}$  distribution at both part- and reco-level. Unfolding network trained to unfold the  $m_t = 169.5\text{GeV}$  sample (Data).

### Narrow features

A particular challenge for any unfolding algorithm is the reconstruction of narrow features that have been smeared out by the forward model. A common example of this is a sharp mass resonance. We illustrate this using the top decay dataset introduced in Ref. [29]. It consists of semi-leptonic  $t\bar{t}$  decays

$$pp \rightarrow t\bar{t} \rightarrow (bqq')(b\ell\nu) + c.c. \quad \text{with } \ell = e, \mu, \tau. \quad (36)$$

The hard-scattering events are generated with Madgraph [64], parton shower and hadronization are simulated with Pythia [53] and finally the detector response with Delphes [55]. Jets are clustered with X Cone [65], both on particle-level and on detector-level. A more detailed description of the simulation and the following event selection is given in Ref. [29].

The goal is to unfold the kinematics of the three subjets originating from the hadronic top-decay. The reconstructed 3-subjet mass  $M_{j_1,j_2,j_3}$  then allows a measurement of the top mass. Past studies [66] identified the choice of top mass used in the simulation as the leading source of systematic uncertainty.

We train our transfer and NIS networks on a simulated sample with a top mass  $m_t = 172.5\text{GeV}$ . We then train SPINUP to unfold a sample with  $m_t = 169.5\text{GeV}$ , the results are shown in Fig. 15. The left plot shows the results on part-level, here we observe that the model learns to recover the correct position for the triple-jet-mass mass peak, but the peak is significantly smeared out compared to the truth distribution. At reco-level, shown in the right plot, SPINUP perfectly recovers the measured data distribution.

This indicates that the method does not struggle with any prior dependence from the simulation top mass, but it does struggle with the degeneracy of the solution space. Due to the large smearing, a wide range of part-level distributions will give rise to almost indistinguishable reco-level distributions. The SPINUP ensemble does not map out the entire space of possible solutions here and underestimates the uncertainty. We attribute this to a preference of neural networks to learn smoother, less peaked functions.

This illustrates a general trade-off in unfolding problems. The SPINUP method is trained via likelihood maximization of the observed reco-data, without imposing any prior on the unfolded distribution. While this is generally a desirable property, in some unfolding problems, such as top mass peaks, we have a strong physics-inspired prior what the distribution should look like. We leave the investigation how to include such knowledge into the method for future work.

## References

- [1] J. M. Campbell *et al.*, *Event generators for high-energy physics experiments*, [SciPost Phys. \*\*16\*\* \(2024\) 5, 130, arXiv:2203.11110 \[hep-ph\]](#).
- [2] S. Badger *et al.*, *Machine learning and LHC event generation*, [SciPost Phys. \*\*14\*\* \(2023\) 4, 079, arXiv:2203.07460 \[hep-ph\]](#).
- [3] I. Brivio, S. Bruggisser, F. Maltoni, R. Moutafis, T. Plehn, E. Vryonidou, S. Westhoff, and C. Zhang, *O new physics, where art thou? A global search in the top sector*, [JHEP \*\*02\*\* \(2020\) 131, arXiv:1910.03606 \[hep-ph\]](#).
- [4] N. Elmer, M. Madigan, T. Plehn, and N. Schmal, *Staying on Top of SMEFT-Likelihood Analyses*, [SciPost Phys. \*\*18\*\* \(2025\) 108, arXiv:2312.12502 \[hep-ph\]](#).
- [5] G. Cowan, *A survey of unfolding methods for particle physics*, [Conf. Proc. C \*\*0203181\*\* \(2002\) 248](#).
- [6] F. Spano, *Unfolding in particle physics: a window on solving inverse problems*, [EPJ Web Conf. \*\*55\*\* \(2013\) 03002](#).
- [7] M. Arratia *et al.*, *Publishing unbinned differential cross section results*, [JINST \*\*17\*\* \(9, 2022\) P01024, arXiv:2109.13243 \[hep-ph\]](#).
- [8] A. Andreassen, P. T. Komiske, E. M. Metodiev, B. Nachman, and J. Thaler, *OmniFold: A Method to Simultaneously Unfold All Observables*, [Phys. Rev. Lett. \*\*124\*\* \(2020\) 18, 182001, arXiv:1911.09107 \[hep-ph\]](#).
- [9] M. Bellagente, A. Butter, G. Kasieczka, T. Plehn, and R. Winterhalder, *How to GAN away Detector Effects*, [SciPost Phys. \*\*8\*\* \(2020\) 4, 070, arXiv:1912.00477 \[hep-ph\]](#).
- [10] A. Andreassen, P. T. Komiske, E. M. Metodiev, B. Nachman, A. Suresh, and J. Thaler, *Scaffolding Simulations with Deep Learning for High-dimensional Deconvolution*, [arXiv:2105.04448 \[stat.ML\]](#).
- [11] K. Datta, D. Kar, and D. Roy, *Unfolding with Generative Adversarial Networks*, [arXiv:1806.00433 \[physics.data-an\]](#).
- [12] J. N. Howard, S. Mandt, D. Whiteson, and Y. Yang, *Foundations of a Fast, Data-Driven, Machine-Learned Simulator*, [arXiv:2101.08944 \[hep-ph\]](#).
- [13] S. Diefenbacher, G.-H. Liu, V. Mikuni, B. Nachman, and W. Nie, *Improving Generative Model-based Unfolding with Schrödinger Bridges*, [arXiv:2308.12351 \[hep-ph\]](#).
- [14] A. Butter, T. Jezo, M. Klasen, M. Kuschick, S. Palacios Schweitzer, and T. Plehn, *Kicking it off(-shell) with direct diffusion*, [SciPost Phys. Core \*\*7\*\* \(2024\) 3, 064, arXiv:2311.17175 \[hep-ph\]](#).
- [15] A. Butter, S. Diefenbacher, N. Huetsch, V. Mikuni, B. Nachman, S. Palacios Schweitzer, and T. Plehn, *Generative Unfolding with Distribution Mapping*, [arXiv:2411.02495 \[hep-ph\]](#).
- [16] M. Bellagente, A. Butter, G. Kasieczka, T. Plehn, A. Rousselot, R. Winterhalder, L. Ardizzone, and U. Köthe, *Invertible Networks or Partons to Detector and Back Again*, [SciPost Phys. \*\*9\*\* \(2020\) 074, arXiv:2006.06685 \[hep-ph\]](#).

- [17] M. Vandegar, M. Kagan, A. Wehenkel, and G. Louppe, *Neural Empirical Bayes: Source Distribution Estimation and its Applications to Simulation-Based Inference*, in *Proceedings of The 24th International Conference on Artificial Intelligence and Statistics*, A. Banerjee and K. Fukumizu, eds. PMLR, 11, 2021. [arXiv:2011.05836 \[stat.ML\]](#).
- [18] M. Backes, A. Butter, M. Dunford, and B. Malaescu, *An unfolding method based on conditional invertible neural networks (cINN) using iterative training*, [SciPost Phys. Core 7 \(2024\) 1, 007](#), [arXiv:2212.08674 \[hep-ph\]](#).
- [19] M. Leigh, J. A. Raine, and T. Golling,  *$\nu$ -Flows: conditional neutrino regression*, [arXiv:2207.00664 \[hep-ph\]](#).
- [20] J. Ackerschott, R. K. Barman, D. Gonçalves, T. Heimel, and T. Plehn, *Returning CP-observables to the frames they belong*, [SciPost Phys. 17 \(2024\) 1, 001](#), [arXiv:2308.00027 \[hep-ph\]](#).
- [21] A. Shmakov, K. Greif, M. Fenton, A. Ghosh, P. Baldi, and D. Whiteson, *End-To-End Latent Variational Diffusion Models for Inverse Problems in High Energy Physics*, [arXiv:2305.10399 \[hep-ex\]](#).
- [22] A. Shmakov, K. Greif, M. J. Fenton, A. Ghosh, P. Baldi, and D. Whiteson, *Full Event Particle-Level Unfolding with Variable-Length Latent Variational Diffusion*, [SciPost Phys. 18 \(2025\) 117](#), [arXiv:2404.14332 \[hep-ex\]](#).
- [23] N. Huetsch *et al.*, *The landscape of unfolding with machine learning*, [SciPost Phys. 18 \(2025\) 2, 070](#), [arXiv:2404.18807 \[hep-ph\]](#).
- [24] L. B. Lucy, *An iterative technique for the rectification of observed distributions*, [Astron. J. 79 \(1974\) 745](#).
- [25] G. D'Agostini, *A Multidimensional unfolding method based on Bayes' theorem*, [Nucl. Instrum. Meth. A362 \(1995\) 487](#).
- [26] A. Hocker and V. Kartvelishvili, *SVD approach to data unfolding*, [Nucl. Instrum. Meth. A372 \(1996\) 469](#), [arXiv:hep-ph/9509307 \[hep-ph\]](#).
- [27] S. Schmitt, *TUnfold: an algorithm for correcting migration effects in high energy physics*, [JINST 7 \(2012\) T10003](#), [arXiv:1205.6201 \[physics.data-an\]](#).
- [28] M. Backes, A. Butter, M. Dunford, and B. Malaescu, *Event-by-event Comparison between Machine-Learning- and Transfer-Matrix-based Unfolding Methods*, [arXiv:2310.17037 \[physics.data-an\]](#).
- [29] L. Favaro, R. Kogler, A. Paasch, S. Palacios Schweitzer, T. Plehn, and D. Schwarz, *How to Unfold Top Decays*, [arXiv:2501.12363 \[hep-ph\]](#).
- [30] H1, V. Andreev *et al.*, *Measurement of lepton-jet correlation in deep-inelastic scattering with the H1 detector using machine learning for unfolding*, [arXiv:2108.12376 \[hep-ex\]](#).
- [31] H1, V. Andreev *et al.*, *Unbinned deep learning jet substructure measurement in high  $Q^2_{ep}$  collisions at HERA*, [Phys. Lett. B 844 \(2023\) 138101](#), [arXiv:2303.13620 \[hep-ex\]](#).
- [32] LHCb, R. Aaij *et al.*, *Multidifferential study of identified charged hadron distributions in Z-tagged jets in proton-proton collisions at  $\sqrt{s} = 13$  TeV*, [Phys. Rev. D 108 \(2023\) L031103](#), [arXiv:2208.11691 \[hep-ex\]](#).

- [33] P. T. Komiske, S. Kryhin, and J. Thaler, *Disentangling quarks and gluons in CMS open data*, *Phys. Rev. D* **106** (2022) 9, 094021, [arXiv:2205.04459 \[hep-ph\]](#).
- [34] STAR, Y. Song, *Measurement of CollinearDrop jet mass and its correlation with SoftDrop groomed jet substructure observables in  $\sqrt{s} = 200$  GeV pp collisions by STAR*, [arXiv:2307.07718 \[nucl-ex\]](#).
- [35] M. R. Buckley and D. Goncalves, *Boosting the Direct CP Measurement of the Higgs-Top Coupling*, *Phys. Rev. Lett.* **116** (2016) 9, 091801, [arXiv:1507.07926 \[hep-ph\]](#).
- [36] J. Ren, L. Wu, and J. M. Yang, *Unveiling CP property of top-Higgs coupling with graph neural networks at the LHC*, *Phys. Lett. B* **802** (2020) 135198, [arXiv:1901.05627 \[hep-ph\]](#).
- [37] B. Bortolato, J. F. Kamenik, N. Košnik, and A. Smolkovič, *Optimized probes of CP -odd effects in the  $t\bar{t}h$  process at hadron colliders*, *Nucl. Phys. B* **964** (2021) 115328, [arXiv:2006.13110 \[hep-ph\]](#).
- [38] H. Bahl, P. Bechtle, S. Heinemeyer, J. Katzy, T. Klingl, K. Peters, M. Saimpert, T. Stefaniak, and G. Weiglein, *Indirect CP probes of the Higgs-top-quark interaction: current LHC constraints and future opportunities*, *JHEP* **11** (2020) 127, [arXiv:2007.08542 \[hep-ph\]](#).
- [39] T. Martini, R.-Q. Pan, M. Schulze, and M. Xiao, *Probing the CP structure of the top quark Yukawa coupling: Loop sensitivity versus on-shell sensitivity*, *Phys. Rev. D* **104** (2021) 5, 055045, [arXiv:2104.04277 \[hep-ph\]](#).
- [40] D. Gonçalves, J. H. Kim, K. Kong, and Y. Wu, *Direct Higgs-top CP-phase measurement with  $t\bar{t}h$  at the 14 TeV LHC and 100 TeV FCC*, *JHEP* **01** (2022) 158, [arXiv:2108.01083 \[hep-ph\]](#).
- [41] R. K. Barman, D. Gonçalves, and F. Kling, *Machine Learning the Higgs-Top CP Phase*, *Phys. Rev. D* **105** (10, 2021) 035023, [arXiv:2110.07635 \[hep-ph\]](#).
- [42] H. Bahl and S. Brass, *Constraining CP-violation in the Higgs-top-quark interaction using machine-learning-based inference*, *JHEP* **03** (10, 2021) 017, [arXiv:2110.10177 \[hep-ph\]](#).
- [43] M. Kraus, T. Martini, S. Peitzsch, and P. Uwer, *Exploring BSM Higgs couplings in single top-quark production*, [arXiv:1908.09100 \[hep-ph\]](#).
- [44] T. Plehn, A. Butter, B. Dillon, T. Heimel, C. Krause, and R. Winterhalder, *Modern Machine Learning for LHC Physicists*, [arXiv:2211.01421 \[hep-ph\]](#).
- [45] A. Butter, T. Heimel, T. Martini, S. Peitzsch, and T. Plehn, *Two invertible networks for the matrix element method*, *SciPost Phys.* **15** (2023) 3, 094, [arXiv:2210.00019 \[hep-ph\]](#).
- [46] T. Heimel, N. Huetsch, R. Winterhalder, T. Plehn, and A. Butter, *Precision-machine learning for the matrix element method*, *SciPost Phys.* **17** (2024) 5, 129, [arXiv:2310.07752 \[hep-ph\]](#).
- [47] T. Heimel, R. Winterhalder, A. Butter, J. Isaacson, C. Krause, F. Maltoni, O. Mattelaer, and T. Plehn, *MadNIS - Neural multi-channel importance sampling*, *SciPost Phys.* **15** (2023) 4, 141, [arXiv:2212.06172 \[hep-ph\]](#).
- [48] T. Heimel, N. Huetsch, F. Maltoni, O. Mattelaer, T. Plehn, and R. Winterhalder, *The MadNIS reloaded*, *SciPost Phys.* **17** (2024) 1, 023, [arXiv:2311.01548 \[hep-ph\]](#).

- [49] T. Heimel, O. Mattelaer, T. Plehn, and R. Winterhalder, *Differentiable MadNIS-Lite*, *SciPost Phys.* **18** (2025) 1, 017, [arXiv:2408.01486 \[hep-ph\]](#).
- [50] Y. Burda, R. Grosse, and R. Salakhutdinov, *Importance weighted autoencoders*, [arXiv:1509.00519 \[cs.LG\]](#).
- [51] A. Butter, N. Huetsch, S. Palacios Schweitzer, T. Plehn, P. Sorrenson, and J. Spinner, *Jet diffusion versus JetGPT – Modern networks for the LHC*, *SciPost Phys. Core* **8** (2025) 026, [arXiv:2305.10475 \[hep-ph\]](#).
- [52] K. Desai, B. Nachman, and J. Thaler, *Moment extraction using an unfolding protocol without binning*, *Phys. Rev. D* **110** (2024) 11, 116013, [arXiv:2407.11284 \[hep-ph\]](#).
- [53] T. Sjöstrand, S. Ask, J. R. Christiansen, R. Corke, N. Desai, P. Ilten, S. Mrenna, S. Prestel, C. O. Rasmussen, and P. Z. Skands, *An introduction to PYTHIA 8.2*, *Comput. Phys. Commun.* **191** (2015) 159, [arXiv:1410.3012 \[hep-ph\]](#).
- [54] J. Bellm *et al.*, *Herwig 7.0/Herwig++ 3.0 release note*, *Eur. Phys. J.* **C76** (2016) 4, 196, [arXiv:1512.01178 \[hep-ph\]](#).
- [55] DELPHES 3, J. de Favereau, C. Delaere, P. Demin, A. Giammanco, V. Lemaître, A. Mertens, and M. Selvaggi, *DELPHES 3, A modular framework for fast simulation of a generic collider experiment*, *JHEP* **02** (2014) 057, [arXiv:1307.6346 \[hep-ex\]](#).
- [56] M. Cacciari, G. P. Salam, and G. Soyez, *The anti- $k_t$  jet clustering algorithm*, *JHEP* **04** (2008) 063, [arXiv:0802.1189 \[hep-ph\]](#).
- [57] M. Cacciari, G. P. Salam, and G. Soyez, *FastJet User Manual*, *Eur. Phys. J. C* **72** (2012) 1896, [arXiv:1111.6097 \[hep-ph\]](#).
- [58] A. J. Larkoski, S. Marzani, G. Soyez, and J. Thaler, *Soft Drop*, *JHEP* **05** (2014) 146, [arXiv:1402.2657 \[hep-ph\]](#).
- [59] M. Dasgupta, A. Fregoso, S. Marzani, and G. P. Salam, *Towards an understanding of jet substructure*, *JHEP* **09** (2013) 029, [arXiv:1307.0007 \[hep-ph\]](#).
- [60] J. Thaler and K. Van Tilburg, *Identifying Boosted Objects with  $N$ -subjettiness*, *JHEP* **03** (2011) 015, [arXiv:1011.2268 \[hep-ph\]](#).
- [61] P. Artoisenet *et al.*, *A framework for Higgs characterisation*, *JHEP* **11** (2013) 043, [arXiv:1306.6464 \[hep-ph\]](#).
- [62] F. Demartin, F. Maltoni, K. Mawatari, and M. Zaro, *Higgs production in association with a single top quark at the LHC*, *Eur. Phys. J. C* **75** (2015) 6, 267, [arXiv:1504.00611 \[hep-ph\]](#).
- [63] K. Cranmer and T. Plehn, *Maximum significance at the LHC and Higgs decays to muons*, *Eur. Phys. J. C* **51** (2007) 415, [arXiv:hep-ph/0605268](#).
- [64] J. Alwall, R. Frederix, S. Frixione, V. Hirschi, F. Maltoni, O. Mattelaer, H. S. Shao, T. Stelzer, P. Torrielli, and M. Zaro, *The automated computation of tree-level and next-to-leading order differential cross sections, and their matching to parton shower simulations*, *JHEP* **07** (2014) 079, [arXiv:1405.0301 \[hep-ph\]](#).
- [65] I. W. Stewart, F. J. Tackmann, J. Thaler, C. K. Vermilion, and T. F. Wilkason, *Xcone:  $N$ -jettiness as an exclusive cone jet algorithm*, *Journal of High Energy Physics* **2015** (Nov., 2015) .

- [66] CMS, A. Tumasyan *et al.*, *Measurement of the differential  $t\bar{t}$  production cross section as a function of the jet mass and extraction of the top quark mass in hadronic decays of boosted top quarks*, *Eur. Phys. J. C* **83** (2023) 7, 560, [arXiv:2211.01456](https://arxiv.org/abs/2211.01456) [hep-ex].